

Attribute2Image: Conditional Image Generation from Visual Attributes

Xinchen Yan¹Jimei Yang²Kihyuk Sohn^{1,3}Honglak Lee¹

¹Computer Science and Engineering Division
University of Michigan, Ann Arbor
{xcyan, kihyuks, honglak}@umich.edu

²Adobe Research
jimyang@adobe.com

³NEC Labs
ksohn@nec-labs.com

Abstract

This paper investigates a problem of generating images from visual attributes. Given the prevalent research for image recognition, the conditional image generation problem is relatively under-explored due to the challenges of learning a good generative model and handling rendering uncertainties in images. To address this, we propose a variety of attribute-conditioned deep variational auto-encoders that enjoy both effective representation learning and Bayesian modeling, from which images can be generated from specified attributes and sampled latent factors. We experiment with natural face images and demonstrate that the proposed models are capable of generating realistic faces with diverse appearance. We further evaluate the proposed models by performing attribute-conditioned image progression, transfer and retrieval. In particular, our generation method achieves superior performance in the retrieval experiment against traditional nearest-neighbor-based methods both qualitatively and quantitatively.

1. Introduction

Image recognition has been extensively studied in computer vision and machine learning. Given an image as input, deep convolutional networks (CNNs) [22, 36, 11, 26, 43, 40, 3, 27, 7, 16, 41] have demonstrated great success in extracting high-level description of images (e.g., object categories, locations, attributes, and captions). However, its inverse problem of generating images from high-level description is relatively under-explored due to challenges of learning a good generative model of images.

In comparison, humans have remarkable ability of generating “mental images” [5, 2] from high-level description. For example, it is almost effortless for people to imagine the picture given the description “I met a young girl with brown hair smiling at me”. We notice that the mental image is built upon a group of visual attributes being extracted from this sentence: (hair color: brown), (gender: female),

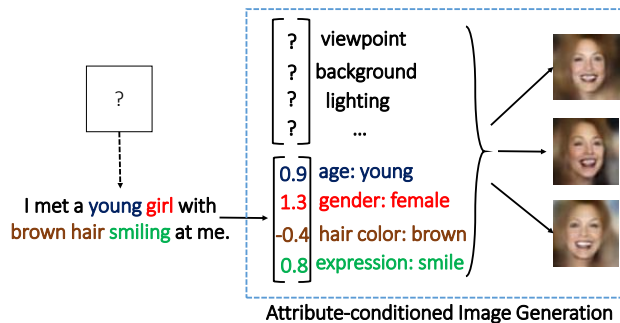


Figure 1. Motivated by the problem of generating images from visual description, we propose techniques for attribute-conditioned image generation.

(age: young) and (expression: smile). Motivated by this, we aim to build a computational model that generates desired picture (the “mental image”) from visual attributes as high-level description, which we call *attribute-conditioned image generation* (Figure 1).

However, the problem of image generation is very challenging due to its non-deterministic characteristic. That is, given fine-grained attribute description, one can find many candidate images satisfying that description by shifting the objects pixel-by-pixel, changing the illumination, or mirroring the images. In fact, if we understand an image as entanglement of different factors of variation, both attribute and unknown (latent) factors will influence the actual pixel-level details. In the example above, the attributes about hair color, gender, age and expression can be inferred from the sentence, but pose, background, and illumination remain unknown as latent factors.

In this paper, we propose a deep neural network for attribute-conditioned image generation. Assuming that latent factors obey a prior distribution where one can draw samples from, the entangled hidden representation is first generated by mingling (via composition) the attributes and sampled latent factors through multilayer perceptrons. Given the entangled representation, local pixels are then generated by a coarse-to-fine convolutional decoder. In or-

der to learn such a neural network in an end-to-end manner, we propose a variety of deep conditional variational auto-encoders (CVAEs) [21]. We extend the CVAE model by introducing edge-aware objective and shape-aware objective. These two objectives act as regularization terms that help to improve the quality of generated images [6].

To evaluate our proposed attribute-conditioned image generation model, we conduct experiments using the Labeled Faces in the Wild (LFW) dataset, which is widely used for face recognition and related applications. Specifically, the classification score of visual attributes (e.g., gender, race, and age) provided by [24] is used as a ground-truth attribute vector to train our conditional generative models. Although these are not hand-annotated and thus are noisy, we found them sufficient to train a good conditional generative model. In experiments, we demonstrate that our model can generate significantly better face images than competing methods (e.g., [8]); our generated images are not only looking more realistic, but also have diverse appearances. Second, we analyze characteristics of the proposed model by performing attribute-conditioned image progression and transfer. Finally, we demonstrate the benefits of the proposed model in attribute-conditioned image retrieval. Compared to traditional image retrieval methods based on nearest neighbor search, our model achieves significantly better performances both qualitatively and quantitatively.

2. Related Work

Generative model is a classic topic in machine learning. As a representative example, the restricted Boltzmann machine (RBM) [33] and its variants [28, 25, 30, 15, 37, 31] have been widely studied for image modeling. The convolutional deep belief network (DBN) [25, 15] has been developed to represent large images by learning hierarchical representations from scratch. Tang and Mohamed [37] presented multi-resolution DBN to model face images at multiple resolutions. Reed et al. [31] introduced a disentangling Boltzmann machine to learn factors of variation such as pose or expression from identity for face images by exploiting higher-order manifold interactions.

In recent years, stochastic feed-forward networks received attention and have been applied to deep generative models [38, 1, 32, 20, 21, 12]. Compared to the models based on Boltzmann machine, the stochastic feed-forward networks entail relatively simple inference as well as easier training. Tang and Salakhutdinov [38] proposed stochastic feed-forward neural networks (SFNNs) with binary stochastic neurons and trained them by maximizing the variational lower bound of the conditional likelihood via generalized EM algorithm. Rezende et al. [32] and Kingma and Welling [20] developed deep latent Gaussian models or variational auto-encoders with an auxiliary recognition network that approximates the intractable posterior of

directed graphical models with Gaussian latent variables. Like SFNNs, the variational lower bound is used as an objective function, but the training process becomes simpler by using the reparameterization trick. Later, Kingma et al. [21] extended the variational auto-encoders to semi-supervised learning with class labels.

In terms of generating realistic and novel images, there are a few recent work [8, 13, 23, 12, 6] that are relevant to ours. Gregor et al. [13] developed recurrent variational auto-encoders with attention mechanism (DRAW) that allow iterative generation of images. Dosovitskiy et al. [8] proposed to generate 3D chairs given graphics code using deep convolutional neural networks, and Kulkarni et al. [23] used variational auto-encoders to model the rendering process of 3D objects. Both of these models [23, 8] assume the existence of a graphics engine during training, from which they have 1) infinite amount of training data and 2) pairs of rendered images that differ only in one factor of variation. Therefore, they are not directly applicable to natural image generation. Recently, the generative adversarial networks (GANs) [12, 10, 6] have been developed for image generation. In the GAN, two models are trained to against each other: a generative model aims to capture the data distribution, while a discriminative model attempts to distinguish between generated samples and training data. The GAN is trained to optimize the min-max objective, which is different from the auto-encoder style training. However, it is known that the training of GAN is relatively more difficult.

Our work can be considered in the context of multimodal learning (e.g., [29, 35, 34]). Ngiam et al. [29] proposed bi-modal deep auto-encoders that are trained to reconstruct or predict multiple modalities from full or partial input observations, respectively. Srivastava and Salakhutdinov [35] developed a multimodal deep Boltzmann machine to learn a shared representation for image and text. Sohn et al. [34] proposed to learn a shared representation of multimodal data via bi-directional conditional prediction by building a conditional prediction model of one data modality given the other, and vice versa. In this context of conditional prediction, modeling the text given the image has recently been tackled with promising results [40, 3, 27, 7, 16, 41]. However, modeling the image given the text has been relatively unexplored. Although not explicitly addressing this problem, our formulation can be potentially applied to conditional image generation directly from the text.

Our work is also related to one line of image editing work [42, 18]. Yang et al. [42] developed an Expression Flow algorithm to transfer the expression from one face image to the other through warping. Kemelmacher-Shlizerman et al. [18] proposed an illumination-aware age progression algorithm to generate faces of a specific person at different ages under same illumination.

3. Attribute-conditioned Variational Auto-encoder

In this section, we describe our proposed probabilistic model for attribute-conditioned image generation. Let X be a collection of images $x \in \mathbb{R}^D$ that are assumed to be generated from the attribute $y \in \mathbb{R}^S$ and latent variable $z \in \mathbb{R}^K$. We further assume that the attribute y and latent variable z are independent, i.e., $p(y, z) = p(y)p(z)$, to exert a better control of the image generation process under different latent variables. Intuitively, attribute y and latent variable z capture different factors of variation and hence this independence assumption is reasonable.

The generation process is as follows: 1) assume attribute y is given, 2) draw a latent variable z from the prior $p(z)$ and 3) generate an image x from $p_\theta(x|y, z)$.

We train our generative model by maximizing the conditional log-likelihood $\log p_\theta(x|y)$. Due to intractable latent variable z , we instead maximize the variational lower bound of conditional log-likelihood by introducing an auxiliary distribution $q_\phi(z|x, y)$ that approximates the true posterior $p_\theta(z|x, y)$ as follows [32, 20, 21]: $\log p_\theta(x|y) =$

$$\begin{aligned} & \mathbb{E}_{q_\phi(z|x, y)} [\log p_\theta(x|y)] \\ &= \mathbb{E}_{q_\phi(z|x, y)} [\log p_\theta(x, z|y) - \log p_\theta(z|x, y)] \\ &= KL(q_\phi(z|x, y) || p_\theta(z|x, y)) \\ & \quad + \underbrace{\mathbb{E}_{q_\phi(z|x, y)} [\log p_\theta(x, z|y) - \log q_\phi(z|x, y)]}_{\triangleq \mathcal{L}_{\text{CVAE}}(x, y; \theta, \phi)}, \end{aligned}$$

and by independence, we have $\mathcal{L}_{\text{CVAE}}(x, y; \theta, \phi) =$

$$-KL(q_\phi(z|x, y) || p_\theta(z)) + \mathbb{E}_{q_\phi(z|x, y)} [\log p_\theta(x|y, z)] \quad (1)$$

We refer the model a conditional variational auto-encoder (CVAE). Here, we assume that the prior $p_\theta(z)$ follows isotropic multivariate Gaussian distribution, while two conditional distributions $p_\theta(x|y, z)$ and $q_\phi(z|x, y)$ are multivariate Gaussian distributions whose mean and covariance are parameterized by $(\mu_\theta(z, y), \sigma_\theta(z, y))$ and $(\mu_\phi(x, y), \sigma_\phi(x, y))$, respectively, i.e.,

$$\begin{aligned} p_\theta(z) &\sim \mathcal{N}(\mathbf{0}, \mathbf{I}) \\ p_\theta(x|y, z) &\sim \mathcal{N}(\mu_\theta(z, y), \sigma_\theta(z, y)) \\ q_\phi(z|x, y) &\sim \mathcal{N}(\mu_\phi(x, y), \sigma_\phi(x, y)) \end{aligned}$$

We refer the auxiliary proposal distribution $q_\phi(z|x, y)$ a recognition model and the conditional data distribution $p_\theta(x|y, z)$ a generation model. Based on these assumptions, the first term in Eq. 1 can be marginalized. We approximate the second term by drawing samples $\{z^{(l)}\}$ from the recognition model $q_\phi(z|x, y)$ as follows:

$$\mathbb{E}_{q_\phi(z|x, y)} [\log p_\theta(x|y, z)] \approx \frac{1}{L} \sum_{l=1}^L \log p_\theta(x|y, z^{(l)}) \quad (2)$$

where $z^{(l)} \sim \mathcal{N}(\mu_\phi(x, y), \sigma_\phi(x, y))$. At training, we apply reparameterization trick on Gaussian latent variable z [20], where $z^{(l)} = g(\mu_\phi(x, y), \sigma_\phi(x, y), \epsilon^{(l)})$, $\epsilon^{(l)} \sim \mathcal{N}(\mathbf{0}, \mathbf{I})$.

Following the VAE framework [20, 21], we construct two Gaussian Multilayer Perceptrons (MLPs) to model the mean and the covariance of the recognition $(\mu_\phi(x, y), \sigma_\phi(x, y))$ and generation $(\mu_\theta(x, y), \sigma_\theta(x, y))$ models (Figure 2(a)). The two terms in Eq. 1 can be simplified as follows:

$$KL = -\frac{1}{2} \sum_{j=1}^K (1 + 2 \log(\sigma_{\phi, j}) - (\mu_{\phi, j})^2 - (\sigma_{\phi, j})^2)$$

$$\log p_\theta(x|y, z^{(l)}) = -\sum_{i=1}^D \left(\log(\sqrt{2\pi}\sigma_{\theta, i}^{(l)}) + \frac{(x_i - \mu_{\theta, i}^{(l)})^2}{2(\sigma_{\theta, i}^{(l)})^2} \right)$$

where $(\mu_\theta^{(l)}, \sigma_\theta^{(l)}) = (\mu_\theta(y, z^{(l)}), \sigma_\theta(y, z^{(l)}))$. During the training, the first term $KL(q_\phi(z|x, y) || p_\theta(z))$ reduces the gap between the prior $p(z)$ and the proposal distribution $q_\phi(z|x, y)$, while the second term $\log p_\theta(x|y, z^{(l)})$ models the input x given the attribute y and the latent variable $z^{(l)}$.

Edge-aware objective. To improve the ‘‘sharpness’’ of the generated samples, we formulate a variant of the CVAE to jointly model image x and the residual image x_e (can be computed by $x_e = x - \text{blur}(x)$, where $\text{blur}(\cdot)$ is a blurring filter) through $p_\theta(x, x_e|y, z)$. It turns out as equivalent to adding an edge-aware objective function \mathcal{L}_e to the original lower bound under certain approximations (details are available in the Appendix A). In other words, we not only model the original image x via $p_\theta(x|y, z)$, but also the residual image x_e through $p_\theta(x_e|y, z)$ as follows:

$$\mathcal{L}_e = \mathbb{E}_{q_\phi(z|x, y)} [\log p_\theta(x_e|y, z)] \sim \frac{1}{L} \sum_{l=1}^L \log p_\theta(x_e|y, z^{(l)}) \quad (3)$$

where $z^{(l)} \sim \mathcal{N}(\mu_\phi(x, y), \sigma_\phi(x, y))$. We model the conditional distribution for x_e as follows:

$$p_\theta(x_e|y, z) = \mathcal{N}(\mu_e(z, y), \mathbf{I}) \quad (4)$$

Note that x_e can be computed from an original image without additional labeling cost. The objective function of an edge-aware CVAE (E-CVAE) can be written as a sum of two objective functions, $\mathcal{L}_{\text{E-CVAE}} = \mathcal{L}_{\text{CVAE}} + \lambda_e \mathcal{L}_e$.

Shape-aware objective. Shape is another important factor of variation for generating images of visual objects besides the content as they are semantically correlated (e.g., female has a long and volume hair). In this section, we thus introduce shape-aware objective function that explicitly enforces our generative model to predict the contents and the

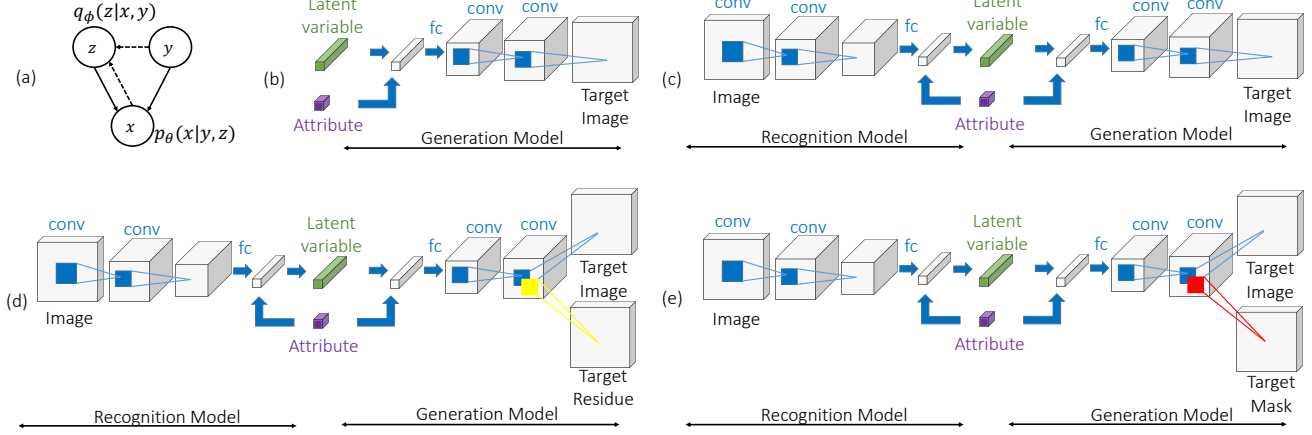


Figure 2. Illustration of model architecture. (a) graphical models of CVAE; (b) SG-CNN architecture; (c) CVAE architecture; (d) edge-aware CVAE architecture; (e) shape-aware CVAE architecture.

corresponding object shape from the attribute and the latent variables at training. This allows the model to jointly infer right pair of shape and contents towards more reasonably-looking image generation. We achieve this by modeling the foreground object mask x_s of an image x :

$$\mathcal{L}_s = \mathbb{E}_{q_\phi(z|x, y)} [\log p_\theta(x_s|y, z)] = \frac{1}{L} \sum_{l=1}^L \log p_\theta(x_s|y, z^{(l)}) \quad (5)$$

where $z^{(l)} \sim \mathcal{N}(\mu_\phi(x, y), \sigma_\phi(x, y))$ and

$$p_\theta(x_s|y, z) = \prod_{j=1}^D \text{Bern}(x_{s,j} | \mu_s(z, y)) \quad (6)$$

Similarly, we combine a shape-aware objective and $\mathcal{L}_{\text{CVAE}}$ to obtain a shape-aware CVAE (S-CVAE) objective function $\mathcal{L}_{\text{S-CVAE}} = \mathcal{L}_{\text{CVAE}} + \lambda_s \mathcal{L}_s$.

Architecture design. As we show in Figure 2(c), the generation network has fully-connected layers followed by convolution layers to generate images from given attribute and latent variables. The fully-connected layers are used for entangling high-level representations, while the stack of convolution and upsampling (followed by non-linearity) is used to generate images in pixel-level.

On the other hand, recognition network has multiple convolution layers followed by fully-connected layers and is used to infer latent variables from the input image and the attribute during the training. The recognition network consists of 4 convolution layers and 3 max-pooling layers with a stride of 2 pixels, followed by 2 fully-connected layers (convolution layers have 64, 128, 256, and 256 channels with kernel size 5×5 , 5×5 , 5×5 , and 3×3 , respectively; the two fully-connected layers have 1024 and 128 neurons). The attribute stream is merged with image stream at the end

of the recognition network. The generation network is designed to be nearly symmetric structure with 2×2 upsampling layers. As we can see in Figure 2(d) and (e), E-CVAE and S-CVAE have additional output streams to residual image and foreground mask, respectively. Please note that recognition network is only used during training. Once the training is done, we can perform the attribute-conditioned image generation with the generation model only.

4. Experiments

We conducted attribute-conditioned image generation experiments on Labeled Faces in the Wild (LFW) dataset, which has more than 13,000 face images collected from the Internet. In our experiments, we aligned the face images using five landmarks [45] and rescaled the center region to 64×64 . We used 73 dimensional attribute scores provided by Kumar et al. [24] that describes different aspects of facial appearance such as age, gender, or facial expression, etc. We used 70% of the data following the training-testing split (View 1), and among training data, 10% were used for cross-validation.

Data preprocessing and augmentation. To make the learning easier, we preprocessed the data by subtracting the global mean and dividing the standard deviation for each color channel. We augment the training data with the following image transformations [22, 9]: 1) flipping images horizontally with probability 0.5, 2) multiplying pixel values of each color channel with a random value $c \in [0.97, 1.03]$, and 3) augmenting the image with its residual with a random tradeoff parameter $s \in [0, 1.5]$. Note that these methods are designed to be invariant to the attribute description.

Implementation details. We use the ADAM stochastic optimization method [19] to train the networks, with mini-

batch of size 32 and the learning rate 0.0003 for all models. The models are implemented using deep learning toolbox MatConvNet [39] and Torch7 [4]. For more visualizations, please refer to the website: <https://sites.google.com/site/attribute2image/>.

4.1. Image Generation: Model Comparisons

For attribute-conditioned image generation, we compare our proposed CVAE model to the generative convolutional neural networks (DG-CNN) [8]. However, there are few drawbacks of DG-CNN such that it requires rich set of attributes (e.g., class label, view point, and additional transformation parameters for chair generation) as an input to generate different images in details, and still the model can only generate a single image for specific set of attributes. As a result, we consider a stronger baseline model that involves stochastic latent variable as an input to the generative CNN, which we call a stochastic generative CNN (SG-CNN). Similarly to the DG-CNN, SG-CNN generates an image using a fixed set of attributes, but also with the latent variables that are randomly drawn from the prior distribution. By doing so, the latent variables can learn other factors of variations in the dataset than those driven by attributes. The objective function of SG-CNN is written as follows:

$$\mathcal{L}_{\text{SG-CNN}} = \frac{1}{L} \sum_{l=1}^L \log p_{\theta}(x|y, z^{(l)}), z^{(l)} \sim \mathcal{N}(\mathbf{0}, \mathbf{I}) \quad (7)$$

Here, we used simple standard normal distribution as prior, but one can easily adopt complicated prior distribution with MLPs. We also note that the SG-CNN can be interpreted as a special case of the CVAE (Eq. 1) whose recognition model is equivalent to the prior model.

For model comparison, we generate samples conditioned on the attribute vectors in the test set with randomly drawn latent variables and visualize them in Figure 3. As we can see, samples generated by the proposed CVAE are qualitatively better looking with rich visual details and diverse viewpoints, whereas those generated by generative CNN models have many artifacts and pixel-level details are significantly blurred. For quantitative evaluation, we compute the conditional log-likelihood (CLL) $\log p(x|y)$ by importance sampling with 50 samples for each attribute vector in the test set (the numbers are computed on the normalized data). The results in Table 1 confirm our visual inspection as the estimated CLL of CVAE is significantly better than those of DG-CNN and SG-CNN.

In sum, the results demonstrate 1) the advantages of formulating attribute-conditioned image generation as a one-to-many mapping task; and 2) an auxiliary recognition network is useful for learning a better generation network.



Figure 3. Qualitative comparison of generated samples by DG-CNN, SG-CNN and baseline CVAE model. Ground-truth images corresponding to the attribute vectors used for each conditional image generation are also visualized.

DG-CNN	SG-CNN	CVAE
-19132.2 ± 26.8	-19562.4 ± 110.8	-6436.4 ± 116.4

Table 1. Test conditional log-likelihood of DG-CNN, SG-CNN and CVAE estimated by importance sampling with 50 samples per attribute (numbers are computed on the normalized data).

4.2. Attribute-conditioned Image Progression

The real-valued attribute vector enables interpolation along each attribute dimension. For example, an image with “smiling” attribute of value 1 is assumed to look more like a smiling face than that of value 0.5. To better analyze the proposed model, we generate images with interpolated attributes by gradually increasing or decreasing the values along each attribute dimension. We regard this process as *attribute-conditioned image progression*. Specifically, for each attribute vector in the test set, we change the value of one attribute dimension by interpolating between the minimum and maximum value. Then, we generate images with $p_{\theta}(x|y, z)$ by interpolating the value of y between the two attribute vectors while keeping latent variable z fixed. For visualization, we use edge-aware CVAE.

As we can see in Figure 4, samples generated by progression are visually consistent with attribute description. By changing attributes like “age”, “gender”, and “race”, the identity-related visual appearance is changed accordingly but the viewpoint, background color, and facial expression are well preserved; on the other hand, by changing attributes like “hair color”, “facial expression”, and “eyewear”, the global appearance is well preserved but the difference appears in the local region. We also visualize the results of progression along two attribute dimensions. As we can see in Figure 5, samples generated by progression change smoothly along two attribute dimensions. These observations demonstrated that the generation process of our model is well controlled by the input attributes.

4.3. Attribute-conditioned Image Transfer

To better understand how the model entangles the latent variable z and attribute y , we design a task that transfers

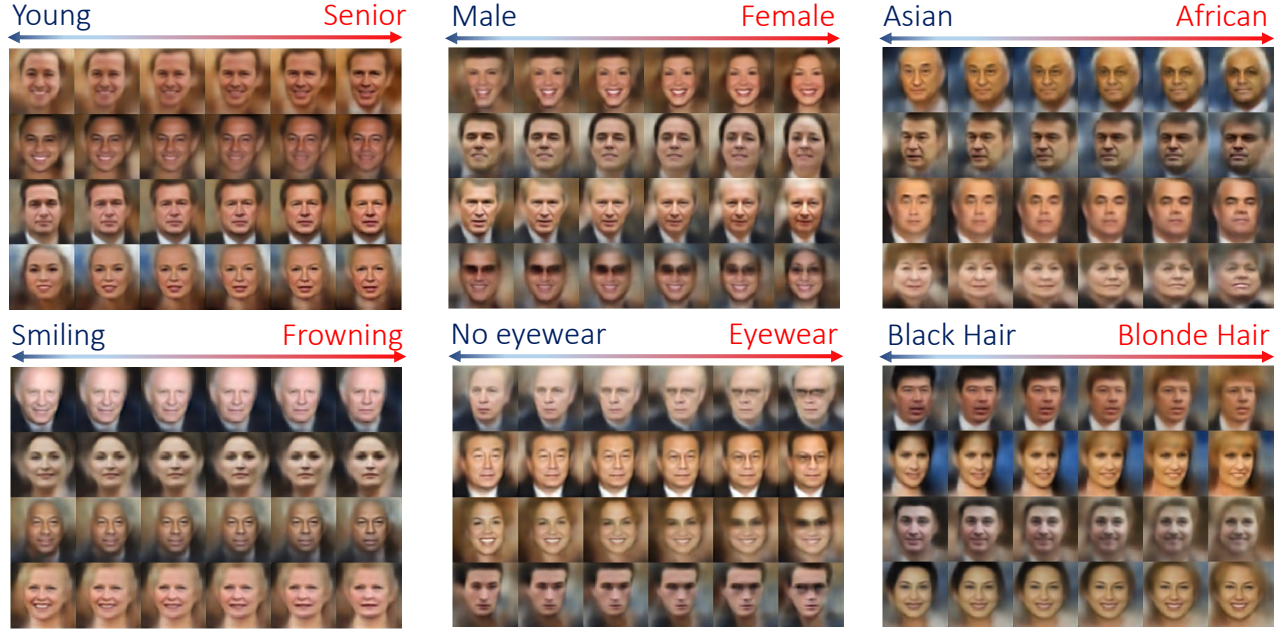


Figure 4. Attribute-conditioned Image Progression (one dimension). The visualization is organized into six attribute groups (e.g., “age”, “gender”, “race”, “facial expression”, “eyewear”, and “hair color”). Within each group, the images are generated from $p_{\theta}(x|y, z)$ with $z \sim \mathcal{N}(0, I)$ and $y = [y_{\alpha}, y_{rest}]$, where $y_{\alpha} = (1 - \alpha) \cdot y_{min} + \alpha \cdot y_{max}$. Here, y_{min} and y_{max} stands for the minimum and maximum attribute value respectively in the dataset along the corresponding dimension.

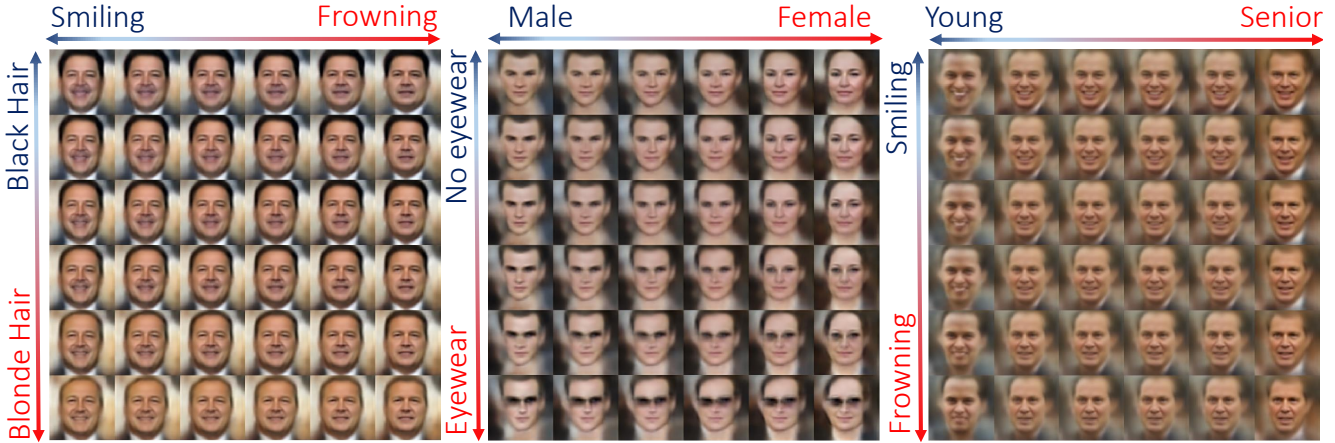


Figure 5. Attribute-conditioned Image Progression (two dimensions)

the attribute from one image to the others while preserving the non-attribute factors. We regard this task as *attribute-conditioned image transfer*. Given a pair of images from the test set, we infer latent variable z from the first image but combined it with the attribute y from the second one. For visualization, we use edge-aware CVAE. As we can see in Figure 6(a)(b), the transferred image 1) shares common pose, illumination and background color with the second input image; 2) looks visually similar to the first input image. These observations suggest that viewpoint, illumination and background color are modeled by the latent factors.

4.4. Attribute-conditioned Image Retrieval

As our model can generate samples from attributes, one practical application is attribute-conditioned image retrieval. Traditional visual attribute-based image retrieval can be done with a nearest neighbor search using a distance metric defined on the attribute vector space, but the performance is often limited by the size of the database. For example, certain combinations of attribute values may not exist in the database but are frequently queried by users. This is a quite common problem in nearest neighbor search since it is very time-consuming and expensive to construct such a huge database with annotations that densely cover

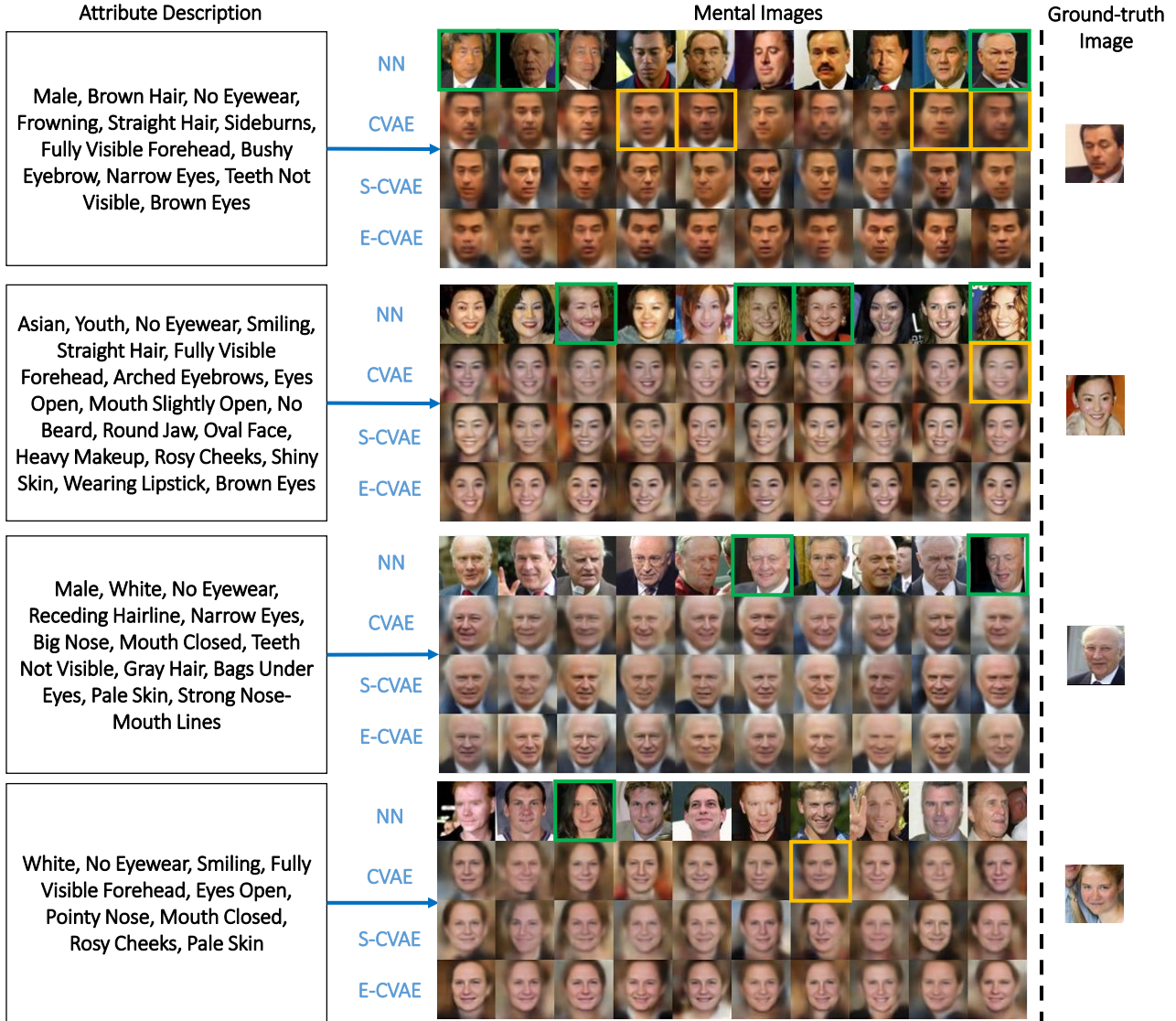


Figure 7. Comparisons on attribute-conditioned image retrieval. The first column lists the attribute description from test set (attributes with values greater than 0.7 are listed). The second column shows the results returned by NN, CVAE, S-CVAE and E-CVAE. The third column shows the ground-truth images from test set. We use yellow boxes to mark the samples that look blurry or have artifacts (nose region), and use green boxes to mark bad samples returned by NN search with one or more attributes mismatched. Note that LFW attribute set only contains Male attribute (but not Female attribute). In other words, images of women have highly negative Male attribute values. For any ground truth image that does not have strong Male attribute value, then it should be viewed as image of Female.

the attribute-label space. Unlike traditional methods, our model can retrieve images by generating images directly from the query attribute vector, reducing the effort to construct a huge database. In this section, we conduct an image retrieval experiment and make a comparison to other methods on LFW dataset. Note that LFW dataset is suitable for experimental comparison since the images are generally sparse w.r.t. the attribute vectors.

Qualitative result. For each query vector, we visualize top-10 images returned from training set by nearest neighbor

search (NN) (Euclidean distance on attribute vector) and 10 images randomly generated by the proposed models (CVAE, S-CVAE, and E-CVAE). As we can see in Figure 7, images generated by the proposed models look more similar to the ground-truth image corresponding to the query attribute vector in the test set than the ones returned by NN. For a specific attribute vector, images generated by our models look non-trivially different from each other, especially for view-point and background color. Moreover, images generated by the edge-aware and shape-aware CVAEs

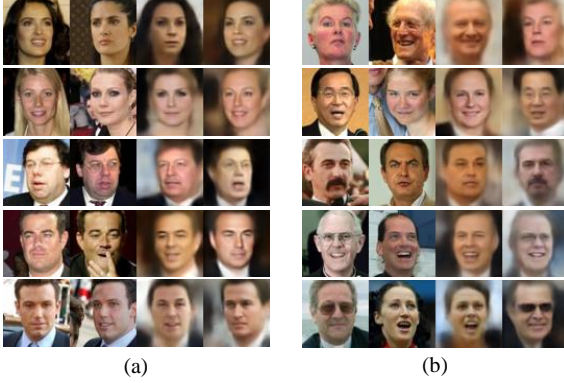


Figure 6. Attribute-conditioned image transfer between (a) the same identity and (b) different identities. For each row, the first two images x_1 and x_2 are the input, the third image x_3 is generated by combining the attribute of the second image y_2 and the latent variable of the first image z_1 , i.e., $x_3 \sim p(x|y_2, z_1)$, and the fourth image x_4 is generated by combining the attribute of the first image y_1 and the latent variable of the second image z_2 , i.e., $x_4 \sim p(x|y_1, z_2)$.

have sharper boundaries at facial objects such as nose or eyes or entire face and hair regions than the ones by the standard CVAE, making them look more realistic.

Quantitative result (pixel similarity). Face images returned by these models have different viewpoints, which makes quantitative analysis difficult. Therefore, we perform frontalization [14, 17] (face regions are detected and normalized to the frontal view) on the faces returned by above-mentioned models. Therefore, we compare the aligned face images in pixel level by cosine similarity. As suggested by Zhu et al. [44], average image of aligned K-nearest neighbors captures better visual similarity to ground-truth than K-nearest neighbors, which we added as a strong baseline (NN_{avg}). Furthermore, to verify that our proposed method does not take unfair advantage in evaluation due to its somewhat blurred image generation, We also add another baseline method by blurring the images returned by NN by a 5×5 average filter (NN_{blur}).

As we can see in Figure 8(a), images retrieved by generation are visually better than the ones returned by variants of nearest neighbor search, which suggests the disadvantages of traditional retrieval method with limited size of database. In addition, the three versions of our model are indistinguishable in terms of similarity score, although the results of the S-CVAE and E-CVAE are visually sharper and cleaner. Interestingly, the blurred images achieve slightly higher similarity score than the original method, which suggests that pixel-level similarity has its limitations.

Quantitative result (attribute similarity). In order to measure the performance quantitatively beyond the pixel-level, we propose to evaluate whether the images returned

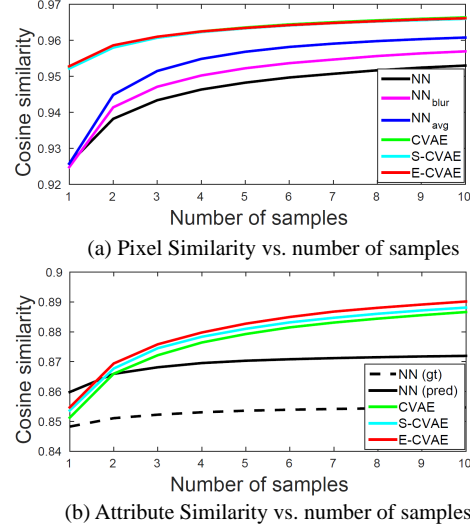


Figure 8. Quantitative evaluations on attribute-conditioned image retrieval. Our CVAE, S-CVAE and E-CVAE are compared with nearest neighbor search (NN), blurred image of nearest neighbor (NN_{blur}) and averaged image of top-K (aligned) nearest neighbors (NN_{avg}) for (a) pixel-level similarity (on frontalized images) and (b) attribute-level similarity between ground-truth and generated samples.

Model	Pixel Similarity	Attribute Similarity
NN	0.9529	0.8719
NN_{blur}	0.9569	0.8292
NN_{avg}	0.9607	NA
SG-CNN	0.9565	0.8293
CVAE	0.9663	0.8866
S-CVAE	0.9659	0.8882
E-CVAE	0.9661	0.8902

Table 2. Quantitative comparisons on attribute-conditioned image retrieval. The best out of 10 samples are evaluated by pixel-level and attribute-level similarities. The attribute-level similarity for NN_{avg} is not available since the attribute regressor is trained on original images of size 64 x 64.

by retrieval really capture the attributes from the query. Therefore, we trained a deep convolutional neural network from scratch as attribute regressor using the image-attribute pairs in the training set. The attribute regressor shares almost the same architecture with the auxiliary recognition model used in generative training. The attribute regressor achieves 14.51 mean squared error (MSE) and 0.98 mean cosine similarity on the test set.

For each attribute vector in the test set, we generate 10 samples and feed them into the attribute regressor. We then compute the cosine similarity between the query attribute and the predicted attributes from generated samples. As a fair comparison, we also compute the cosine similarity between the query attribute and the predicted attributes from nearest neighbor samples.

As we can see in Figure 8(b), samples generated by the proposed CVAE model reflect the attribute better than baseline methods like SG-CNN and nearest neighbor search. In addition, the attribute of samples returned by nearest neighbor search is more accurate than the ones after applying average filter. This suggests that sharper images are more discriminative for attribute prediction. This also strengthens the observation (see Figure 7) that samples generated from S-CVAE and E-CVAE reflect the attribute better than CVAE. We summarize the quantitative results in Table 2. More evaluations are available in Appendix B.

5. Conclusion

We introduced a problem of generating images from visual attributes. To learn such generation process, we proposed a variety of deep conditional variational auto-encoders. By comparing generated samples, our model demonstrated its advantages both qualitatively and quantitatively over baseline approaches. We also evaluated our model by performing attribute-conditioned image progression and transfer. The practical value of our model is further demonstrated through attribute-conditioned image retrieval with superior performance over nearest neighbor search.

References

- [1] Y. Bengio, E. Thibodeau-Laufer, G. Alain, and J. Yosinski. Deep generative stochastic networks trainable by backprop. *arXiv preprint arXiv:1306.1091*, 2013.
- [2] A. Chang, W. Monroe, M. Savva, C. Potts, and C. D. Manning. Text to 3D scene generation with rich lexical grounding. *arXiv preprint arXiv:1505.06289*, 2015.
- [3] X. Chen and C. L. Zitnick. Minds eye: A recurrent visual representation for image caption generation. In *CVPR*, 2015.
- [4] R. Collobert, K. Kavukcuoglu, and C. Farabet. Torch7: A matlab-like environment for machine learning. In *BigLearn, NIPS Workshop*, 2011.
- [5] B. Coyne and R. Sproat. Wordseye: an automatic text-to-scene conversion system. In *SIGGRAPH*, 2001.
- [6] E. Denton, S. Chintala, A. Szlam, and R. Fergus. Deep generative image models using a Laplacian pyramid of adversarial networks. In *NIPS*, 2015.
- [7] J. Donahue, L. A. Hendricks, S. Guadarrama, M. Rohrbach, S. Venugopalan, K. Saenko, and T. Darrell. Long-term recurrent convolutional networks for visual recognition and description. In *CVPR*, 2015.
- [8] A. Dosovitskiy, J. T. Springenberg, and T. Brox. Learning to generate chairs with convolutional neural networks. In *CVPR*, 2015.
- [9] D. Eigen, C. Puhrsch, and R. Fergus. Depth map prediction from a single image using a multi-scale deep network. In *NIPS*, 2014.
- [10] J. Gauthier. Conditional generative adversarial nets for convolutional face generation. Technical report, 2015.
- [11] R. Girshick, J. Donahue, T. Darrell, and J. Malik. Rich feature hierarchies for accurate object detection and semantic segmentation. In *CVPR*, 2014.
- [12] I. Goodfellow, J. Pouget-Abadie, M. Mirza, B. Xu, D. Warde-Farley, S. Ozair, A. Courville, and Y. Bengio. Generative adversarial nets. In *NIPS*, 2014.
- [13] K. Gregor, I. Danihelka, A. Graves, and D. Wierstra. DRAW: A recurrent neural network for image generation. In *ICML*, 2015.
- [14] T. Hassner, S. Harel, E. Paz, and R. Enbar. Effective face frontalization in unconstrained images. In *CVPR*, 2015.
- [15] G. B. Huang, H. Lee, and E. Learned-Miller. Learning hierarchical representations for face verification with convolutional deep belief networks. In *CVPR*, 2012.
- [16] A. Karpathy and L. Fei-Fei. Deep visual-semantic alignments for generating image descriptions. In *CVPR*, 2015.
- [17] V. Kazemi and J. Sullivan. One millisecond face alignment with an ensemble of regression trees. In *CVPR*, 2014.
- [18] I. Kemelmacher-Shlizerman, S. Suwajanakorn, and S. M. Seitz. Illumination-aware age progression. In *CVPR*, 2014.
- [19] D. Kingma and J. Ba. ADAM: A method for stochastic optimization. In *ICLR*, 2015.
- [20] D. P. Kingma and M. Welling. Auto-encoding variational Bayes. In *ICLR*, 2014.
- [21] D. P. Kingma, S. Mohamed, D. J. Rezende, and M. Welling. Semi-supervised learning with deep generative models. In *NIPS*, 2014.
- [22] A. Krizhevsky, I. Sutskever, and G. E. Hinton. Imagenet classification with deep convolutional neural networks. In *NIPS*, 2012.

- [23] T. D. Kulkarni, W. Whitney, P. Kohli, and J. B. Tenenbaum. Deep convolutional inverse graphics network. In *NIPS*, 2015.
- [24] N. Kumar, A. C. Berg, P. N. Belhumeur, and S. K. Nayar. Attribute and simile classifiers for face verification. In *ICCV*, 2009.
- [25] H. Lee, R. Grosse, R. Ranganath, and A. Y. Ng. Convolutional deep belief networks for scalable unsupervised learning of hierarchical representations. In *ICML*, 2009.
- [26] J. Long, E. Shelhamer, and T. Darrell. Fully convolutional networks for semantic segmentation. In *CVPR*, 2015.
- [27] J. Mao, W. Xu, Y. Yang, J. Wang, and A. Yuille. Deep captioning with multimodal recurrent neural networks (M-RNN). In *ICLR*, 2015.
- [28] R. Memisevic and G. Hinton. Unsupervised learning of image transformations. In *CVPR*, 2007.
- [29] J. Ngiam, A. Khosla, M. Kim, J. Nam, H. Lee, and A. Y. Ng. Multimodal deep learning. In *ICML*, 2011.
- [30] M. Ranzato, J. Susskind, V. Mnih, and G. Hinton. On deep generative models with applications to recognition. In *CVPR*, 2011.
- [31] S. Reed, K. Sohn, Y. Zhang, and H. Lee. Learning to disentangle factors of variation with manifold interaction. In *ICML*, 2014.
- [32] D. J. Rezende, S. Mohamed, and D. Wierstra. Stochastic backpropagation and approximate inference in deep generative models. In *ICML*, 2014.
- [33] P. Smolensky. Information processing in dynamical systems: Foundations of harmony theory. In D. E. Rumelhart and J. L. McClelland, editors, *Parallel Distributed Processing: Volume 1*. 1986.
- [34] K. Sohn, W. Shang, and H. Lee. Improved multimodal deep learning with variation of information. In *NIPS*, 2014.
- [35] N. Srivastava and R. R. Salakhutdinov. Multimodal learning with deep Boltzmann machines. In *NIPS*, 2012.
- [36] C. Szegedy, W. Liu, Y. Jia, P. Sermanet, S. Reed, D. Anguelov, D. Erhan, V. Vanhoucke, and A. Rabinovich. Going deeper with convolutions. In *CVPR*, 2015.
- [37] Y. Tang and A.-R. Mohamed. Multiresolution deep belief networks. In *AISTATS*, 2012.
- [38] Y. Tang and R. Salakhutdinov. Learning stochastic feedforward neural networks. In *NIPS*, 2013.
- [39] A. Vedaldi and K. Lenc. Matconvnet-convolutional neural networks for MATLAB. *arXiv preprint arXiv:1412.4564*, 2014.
- [40] O. Vinyals, A. Toshev, S. Bengio, and D. Erhan. Show and tell: A neural image caption generator. In *CVPR*, 2015.
- [41] K. Xu, J. Ba, R. Kiros, A. Courville, R. Salakhutdinov, R. Zemel, and Y. Bengio. Show, attend and tell: Neural image caption generation with visual attention. In *ICML*, 2015.
- [42] F. Yang, J. Wang, E. Shechtman, L. Bourdev, and D. Metaxas. Expression flow for 3D-aware face component transfer. In *SIGGRAPH*, 2011.
- [43] B. Zhou, A. Lapedriza, J. Xiao, A. Torralba, and A. Oliva. Learning deep features for scene recognition using places database. In *NIPS*, 2014.
- [44] J.-Y. Zhu, Y. J. Lee, and A. A. Efros. Averageexplorer: Interactive exploration and alignment of visual data collections. *ACM Transactions on Graphics (TOG)*, 33(4):160, 2014.
- [45] S. Zhu, C. Li, C. C. Loy, and X. Tang. Transferring landmark annotations for cross-dataset face alignment. *arXiv preprint arXiv:1409.0602*, 2014.

A. Derivation of Edge-aware CVAE Objective

We provide a detailed derivation of the objective function for edge-aware CVAE (E-CVAE). Similarly to the standard CVAE, we have x as input image, y as attribute labels, and z as latent variables. In addition, we have x_e as another input modality for E-CVAE. The joint conditional log-likelihood of x and x_e given y can be written as follows:

$$\begin{aligned} & \log p_\theta(x, x_e|y) \\ &= \mathbb{E}_{q_\phi(z|x_e, y)} [\log p_\theta(x, x_e|y)] \\ &= \mathbb{E}_{q_\phi(z|x, x_e, y)} [\log p_\theta(x, x_e, z|y) - \log p_\theta(z|x, x_e, y)] \\ &= KL(q_\phi(z|x, x_e, y) || p_\theta(z|x, x_e, y)) \\ &\quad + \underbrace{\mathbb{E}_{q_\phi(z|x, x_e, y)} [\log p_\theta(x, x_e, z|y) - \log q_\phi(z|x, x_e, y)]}_{\triangleq \mathcal{L}_{\text{E-CVAE}}(x, x_e, y; \theta, \phi)}, \end{aligned} \quad (8)$$

and by independence of y and z , we have

$$\begin{aligned} \mathcal{L}_{\text{E-CVAE}}(x, x_e, y) &= -KL(q_\phi(z|x, x_e, y) || p_\theta(z)) \\ &\quad + \mathbb{E}_{q_\phi(z|x, x_e, y)} [\log p_\theta(x, x_e|y, z)] \end{aligned} \quad (9)$$

For presentation clarity, we omit model parameters (θ, ϕ) from objective functions. Here, we simplify the recognition model $q_\phi(z|x, x_e, y)$ into $q_\phi(z|x, y)$ under the assumption that the residual image x_e can be directly derived from the input image x . For generation model, however, we doesn't make such an assumption and let the model to predict both original and the residual images from attribute y and the latent variables z . We further assume conditional independence of x and x_e , i.e.,

$$\log p_\theta(x, x_e|y, z) = \log p_\theta(x|y, z) + \log p_\theta(x_e|y, z) \quad (10)$$

To make the formulation more flexible, we add a tuning knob λ_e for \mathcal{L}_e , which completes the derivation for the following objective function:

$$\mathcal{L}_{\text{E-CVAE}}(x, x_e, y) = \mathcal{L}_{\text{CVAE}}(x, y) + \lambda_e \mathcal{L}_e(x_e, y) \quad (11)$$

B. More evaluations on attribute similarity

To better understand the difference between CVAE models, we evaluate the attribute similarities (i.e., cosine similarity between attribute vectors) of the images generated by the CVAE, S-CVAE, and E-CVAE on the subset of attributes.¹ Specifically, we selected 6 eyes-related, 4 mouth-related, 17 hair-related, and 19 detail-related attributes from 73 facial attributes, and summarized them in Table 3. As we can see in Table 4, images generated by the E-CVAE achieve higher similarity scores on attributes that are related to face parts (e.g., eye, mouth) and the facial detail

¹We follow the experimental procedure described in Section 4.4. Quantitative result (attribute similarity) of the main text.

subset (#)	attribute names
eyes (6)	<i>bushy eyebrows, arched eyebrows, narrow eyes, eyes open, bags under eyes, brown eyes</i>
mouth (4)	<i>mouth closed, mouth slightly open, mouth widely open, and teeth not visible</i>
detail (19)	<i>bushy eyebrows, arched eyebrows, narrow eyes, eyes open, bags under eyes, brown eyes, big nose, pointy nose, teeth not visible, mouth slightly open, mouth widely open, round jaw, double chin, rosy cheeks, mouth closed, wearing lipstick, flushed face, strong nose-mouth lines, high cheekbones</i>
hair (17)	<i>black hair, blonde hair, brown hair, gray hair, bald, curly hair, wavy hair, straight hair, receding hairline, bangs, sideburns, mustache, no beard, goatee, fully visible forehead, partially visible forehead, obstructed forehead, 5 o'clock shadow</i>

Table 3. Subset of facial attributes with related categories.

attributes, while the S-CVAE shows strong performance on hair-related attributes. This aligns with our qualitative results where the images generated by the E-CVAE have sharper edges compared to other CVAE models, and those generated by the S-CVAE can preserve more shape information, e.g., hair shape.

subset (#)	NN (pred)	CVAE	S-CVAE	E-CVAE
eyes (6)	0.6921	0.6987	0.6894	0.7083
mouth (4)	0.7488	0.7813	0.7867	0.8055
detail (19)	0.7901	0.8105	0.8079	0.8158
hair (17)	0.7626	0.8020	0.8034	0.7963
all (73)	0.8342	0.8514	0.8531	0.8556

Table 4. Attribute similarity on different subsets of attributes.

We also conduct the pairwise t-test on the attribute similarity scores returned by different models. As we can see in Table 5, the results is consistent with our claim that S-CVAE and E-CVAE improve upon the baseline CVAE not only visually, but also in terms of attribute similarity.

	NN (pred)	CVAE	S-CVAE	E-CVAE
NN (pred)	–	(0, 1)	(0, 1)	(0, 1)
CVAE	(1, 0)	–	(0, 0.999)	(0, 1)
S-CVAE	(1, 0)	(1, 5e ⁻⁶)	–	(0, 1)
E-CVAE	(1, 0)	(1, 1e ⁻²²)	(1, 2e ⁻⁹)	–

Table 5. Pairwise t-test on the cosine similarity of different models. For each pair of methods, we conduct the single-tail t-test (right-tail test) on the cosine similarity; we report (h, p) , where h is the t-test result of the null hypothesis and p is the p-value. Intuitively speaking, for the ij -th entry, $h = 1$ with low p-value (< 0.05) means that the method i consistently gives higher results than the method j with statistical significance.